# Galilean-invariant lattice-Boltzmann simulation of liquid-vapor interface dynamics

A. N. Kalarakis, V. N. Burganos,* and A. C. Payatakes
*Institute of Chemical Engineering and High Temperature Chemical Processes—Foundation for Research and Technology, Hellas (ICE/HT-FORTH), P.O. Box 1414, GR 265 04 Patras, Greece*
*and Department of Chemical Engineering, University of Patras, P.O. Box 1414, GR 265 04 Patras, Greece*
(Received 23 July 2001; revised manuscript received 1 February 2002; published 23 April 2002)

A two-dimensional two-phase lattice-Boltzmann model is presented and used for the study of interfacial phenomena under static and flow conditions. The model is based on the nonideal lattice-Boltzmann model proposed originally by Swift, Osborn, and Yeomans [Phys. Rev. Lett. **75**, 830 (1995)] and makes it possible to couple a prescribed equation of state with the pressure tensor at the interface and the excess free-energy density formalism. The characteristic feature of the present model is that Galilean invariance is restored in the presence of interfaces without sacrificing any of the merits of the original model and, hence, the Navier-Stokes equation is adequately (to second order) recovered. The fluid properties can be prescribed in a thermodynamically consistent manner, which remains accurate at states close to the critical point. The model is first validated through static equilibrium tests and then applied to flow systems. It is shown that the simulator can reproduce some known two-phase flow configurations, like the motion of deformable droplets under the action of an external flow field. The simulator can also capture some interesting events during jet breakup and can be useful for the parametric study of the process in the two-dimensional case.

DOI: 10.1103/PhysRevE.65.056702 PACS number(s): 83.85.Pt, 68.03.Cd, 83.50.−v

## I. INTRODUCTION

Lattice-Boltzmann (LB) methods have provided a powerful alternative to traditional numerical techniques for the study of equilibrium and dynamic properties of fluid systems. Since the first attempts to simulate hydrodynamic phenomena using lattice-gas (LG) automata by Frisch, Hasslacher, and Pomeau (FHP) [1], numerous publications have appeared in this area, reflecting very intensive research efforts in mesoscopic simulations of fluid systems. The initial drawbacks of numerical noise, non-Galilean invariance, and velocity dependent pressure of the lattice-gas methods were later addressed successfully in the lattice-Boltzmann method. The LG Boolean variables and the Fermi-Dirac equilibrium distribution function [2] have been replaced by single-particle distribution functions and Boltzmann statistics [3,4]. Furthermore, the collision operator formulation was replaced by the single relaxation time approximation, introduced initially by Bhatnagar, Gross, and Krook (BGK) [5], which simplified considerably the LB formulation and numerical computations.

LG and LB models proved very useful in the particular case of two-phase flow due to both the complexity encountered when traditional techniques were to be employed in the interface region and the strong scientific and technological interest of multiphase systems. Rothman and Keller [6] proposed a two-component LG model, whereas Gustensen and co-workers [7,8] employed Boltzmann statistics in their model introducing, thus, a multiphase LB model. Modifications to account for different viscosities and rest particle populations in the two phases and to satisfy the standard interfacial conditions at first order were proposed by Ginzbourg and Adler [9]. Grunau and co-workers [10,11] simplified their model by replacing the collision operator with a single-time relaxation factor. In these models, phase separation is achieved through a phenomenological ''antidiffusion'' potential, which can be somehow connected to the interfacial tension. Appert and co-workers [12,13] proposed a two-phase LG model, which was based on the basic LG single-phase model with the additional feature of allowing for momentum exchange between remote particles. The interaction of those particles eventually leads to phase transition. The momentum exchange is dictated either by a simple set of rules, based mainly on the distance of particles considered in pairs, or by more complicated rules, applied to the entire particle ensemble. Shan and Chen [14] proposed an alternative approach: a special microscopic interaction affecting nearest neighbors only can be shown to correspond to a nonideal equation of state, allowing thus for coexistence of two or more phases. A temperaturelike parameter is involved in the modeling of the phase transition.

Swift and co-workers [15,16] proposed a LB model for isothermal two-phase systems, using a Cahn-Hilliard [17] type of approach for phase transition. The system reaches equilibrium when the free-energy functional, quantified according to the van der Waals square-gradient approximation [18], is minimized. The interfacial phenomena are controlled by the pressure tensor, suitably formulated for nonideal fluids, whereas the surface tension is expressed according to the van der Waals theory of capillarity. Angelopoulos *et al.* [19] introduced a methodology for the prescription of the fluid properties in this LB model and applied it to two-phase flow problems, such as drainage and imbibition in porous media, under various wettability conditions.

Recent LB multiphase techniques have adopted the direct discretization of the full Boltzmann equation, initially proposed by He and Luo [20], Luo [21], and, independently, by Abe [22]. In order to account for the nonideality of dense gases, the extended Boltzmann equation, as initially proosed

*Corresponding author. Email address: vbur@iceht.forth.gr

 

by Enskog [23], should be used. Including terms that become non-negligible for dense fluids [21], such as the volume exclusion corrections, the extended discrete Boltzmann equation leads to a nonideal state equation, which allows for phase coexistence. In addition, He, Shan, and Doolen [24] have proposed a slightly different scheme based on the discrete Boltzmann equation, assuming that the velocity derivative of the nonequilibrium distribution functions ($\nabla_c f^{\mathrm{neq}}$) can be neglected. The force in the Boltzmann equation is made up of two contributions, namely, the mean force on each particle due to the intermolecular attraction and the force associated with the volume exclusion effect (Enskog analysis [23]). Consideration of these two factors leads to a nonideal equation of state.

In this work, an improvement of the single-component two-phase seven-bit LB model by Swift, Osborn, and Yeomans [15] and Angelopoulos *et al.* [19] is proposed and used to simulate droplet formation and droplet motion under an external flow field. A potential weakness of the original model, as has been already pointed out [16,21], is the lack of Galilean invariance. Because of that, transient or steady state flow simulations may lead to reduced accuracy in the calculation of the flow field or in the shape and velocity of moving droplets. Nevertheless, it is shown here that Galilean invariance can be restored, to second-order accuracy, using a new formulation for the definition of the zero-order momentum flux tensor. A similar approach to restore Galilean invariance in the nine-bit model [25] has demonstrated greatly improved performance during simulation of Couette flow, and shear and translation of a droplet. Inamuro, Konishi, and Ogino [26] used an asymptotic analysis to restore Galilean invariance also in the nine-bit model.

This paper is organized as follows. Section II presents an outline of the original model in two-dimensions (2D) along with an algorithm for the step-by-step prescription of the fluid properties. The model and the details of the formulation that restores Galilean invariance are also presented there. Section III shows the results of the applications of the model to static and flow problems, including jet breakup and droplet formation. The main conclusions of this work are summarized in Sec. IV.

## II. LATTICE-BOLTZMANN TWO-PHASE MODEL

The lattice-Boltzmann equation in view of the BGK approximation is

$$f_i(\underline{x}+\underline{e}_i,t+1)=f_i(\underline{x},t)-\frac{f_i(\underline{x},t)-f_i^{\mathrm{eq}}(\underline{x},t)}{\tau}, \tag{1}$$

where $\tau$ is the relaxation time and subscript $i$ indicates the link direction in a single cell ($i=0,1,\ldots,b$; $b$ being the number of links from a node to its nearest neighbors and 0 indicating rest population).

Swift, Osborn, and Yeomans [15] proposed the following expansion of the equilibrium distribution function for use with two-phase systems:

$$f_i^{\mathrm{eq}}=A+B(\underline{e}_i\cdot\underline{u})+C(\underline{e}_i\cdot\underline{u})^2+D\underline{u}^2+\underline{\underline{G}}:\underline{e}_i\underline{e}_i+\underline{F}\underline{e}_i, \tag{2a}$$

$$f_0^{\mathrm{eq}}=A_0+D_0u^2. \tag{2b}$$

The coefficients for the 2D hexagonal lattice are given by

$$A_0=\rho-2(p_0-m\rho\nabla^2\rho)=\rho-6A,\quad A=\frac{p_0-m\rho\nabla^2\rho}{3}, \tag{3a}$$

$$B=\rho/3, \tag{3b}$$

$$C=2\rho/3, \tag{3c}$$

$$D_0=-\rho,\quad D=-\rho/6, \tag{3d}$$

$$G_{xx}=\frac{m}{3}\left[\left(\frac{\partial\rho}{\partial x}\right)^2-\left(\frac{\partial\rho}{\partial y}\right)^2\right]=-G_{yy},\quad G_{xy}=\frac{2m}{3}\frac{\partial\rho}{\partial x}\frac{\partial\rho}{\partial y}, \tag{3e}$$

$$F_x=F_y=0, \tag{3f}$$

where $\rho$ is density and $m$ a fluid parameter (see below).

### A. Prescription of the fluid properties

Using the basic equilibrium equations for a van der Waals fluid, Angelopoulos *et al.* [19] derived useful expressions for the density variation across the interface between the gas and liquid phases. The correlation between the interface thickness $D$ and the equilibrium fluid densities is given by

$$m=\frac{3D\sigma}{2(\rho_l-\rho_g)^2}, \tag{4}$$

where $\sigma$ is the interfacial tension, expressed as

$$\sigma=m\int_{-\infty}^{\infty}\left(\frac{\partial(\rho(z))}{\partial z}\right)^2dz \tag{5}$$

in the van der Waals theory.

The kinematic viscosity within the interface region is approximated by

$$\nu(\rho)=\frac{(\nu_l-\nu_g)\rho+\nu_g\rho_l-\nu_l\rho_g}{\rho_l-\rho_g}, \tag{6}$$

where $\nu_l$ and $\nu_g$ are the kinematic viscosities of the liquid and vapor phases, respectively, and relate to the corresponding relaxation time constants through

$$\nu_j=\frac{2\tau_j-1}{8},\quad j=l,g. \tag{7}$$

It is shown that the mass and momentum conservation equations for the fluid are the following:

Mass conservation equation,

$$\frac{\partial}{\partial t}\rho+\nabla\cdot\rho\underline{u}=0. \tag{8}$$

Momentum conservation equation,

$$\frac{\partial}{\partial t}(\rho\underline{u})+\nabla\cdot(\rho\underline{u}\underline{u})=-\nabla\underline{\underline{P}}+\nabla\left[\left(\frac{2\tau-1}{8}\right)\rho\{\nabla\underline{u}+(\nabla\underline{u})^{\tau}\}\right]+\nabla\left[\left(\tau-\frac{1}{2}\right)\left(\frac{1}{4}-\frac{\partial P}{\partial\rho}\right)\rho(\nabla\cdot\underline{u})\right]+\nabla\left[\left(\frac{2\tau-1}{8}\right)\left(1-\frac{1}{4}\frac{\partial P}{\partial\rho}\right)\{\underline{u}\nabla\rho+(\underline{u}\nabla\rho)^{\tau}\}\right]+\nabla\left[\left(\tau-\frac{1}{2}\right)\left(\frac{1}{4}-\frac{\partial P}{\partial\rho}\right)\times(\underline{u}\cdot\nabla\rho)\right]+O(u^3), \tag{9}$$

where the equation $\partial_\alpha P_{\alpha\beta}=\partial_\rho P\partial_\alpha\rho$ was used, with $\rho$ and $\rho\underline{u}$ the macroscopic local density and momentum density, respectively,

$$\rho=\sum_i f_i^{\mathrm{eq}}, \tag{10}$$

$$\rho\underline{u}=\sum_i \underline{e}_i f_i^{\mathrm{eq}}. \tag{11}$$

In Eq. (9), $\underline{\underline{P}}$ is the pressure tensor for a nonuniform fluid [27],

$$\underline{\underline{P}}=P\underline{\underline{\delta}}+m\nabla\rho\nabla\rho,$$

or

$$\underline{\underline{P}}=\left(p_0-m\rho\nabla^2\rho-\frac{m}{2}\left|\nabla\rho\right|^2\right)\underline{\underline{\delta}}+m\nabla\rho\nabla\rho, \tag{12}$$

where $p_0$ is the fluid pressure, connected to the temperature through the equation of state, and $m$ is the parameter that enters the expression for the free-energy functional according to the square-gradient approximation,

$$F[\rho(\underline{r})]=\int dr[\tfrac{1}{2}m|\nabla\rho(\underline{r})|^2+\tilde{\psi}(\rho(\underline{r}))]. \tag{13}$$

In Eq. (13), $\tilde{\psi}(\rho)$ is the local free-energy density of the fluid of uniform density $\rho$.

Comparing Eq. (9) with the actual Navier-Stokes equation,

$$\frac{\partial}{\partial t}(\rho\underline{u})+\nabla\cdot(\rho\underline{u}\underline{u})=-\nabla P+\nabla\cdot[\mu\{\nabla\underline{u}+(\nabla\underline{u})^{\tau}\}]+\nabla[(\kappa-\mu)\nabla\cdot\underline{u}]+\rho\underline{g}, \tag{14}$$

the kinematic viscosity $\nu$ and the bulk viscosity $\kappa$ can be identified, as

$$\nu=\frac{2\tau-1}{8}, \tag{15a}$$

$$\frac{\kappa}{\rho}=2\left(1-2\frac{\partial P}{\partial\rho}\right)\nu. \tag{15b}$$

The LB momentum equation resembles closely the Navier-Stokes equation except for the last two terms, which contain density gradients and may, thus, be responsible for the lack of Galilean invariance. The usual assumption made in single-phase systems, namely, that these additional terms are of order $O(u^3)$—since density gradients are $O(u^2)$—and, therefore, are negligible [28], is not valid for multiphase systems. The density gradients may obtain large values within the interface region, depending on the interface thickness and the bulk density difference. As it will be shown below, if these effects are not accounted for properly by restoring Galilean invariance, they may lead to very erroneous results.

In index notation, the LB motion equation assumes the following form:

$$\partial_t(\rho u_\alpha)+\partial_\beta(\rho u_\alpha u_\beta)=-\partial_\alpha P_{\alpha\beta}+\partial_\beta[\nu\rho(\partial_\alpha u_\beta+\partial_\beta u_\alpha)]+\partial_\beta\left(\nu'\sum_\gamma \partial_\gamma\rho u_\gamma\delta_{\alpha\beta}\right)+\partial_\beta[\nu'(u_\beta\partial_\alpha\rho+u_\alpha\partial_\beta\rho)]. \tag{16}$$

The symbols $\partial_\beta$ and $\partial_t$ represent the spatial and time derivatives, respectively, and $\nu'$ is given by

$$\nu'=\nu\left(1-4\frac{\partial P}{\partial\rho}\right). \tag{17}$$

In order to restore the Galilean invariance, the last two terms of Eq. (16) must be eliminated. A way to achieve this is by merging them into the pressure term, which should then have the following form:

$$P'_{\alpha\beta}=P_{\alpha\beta}+\zeta(u_\beta\partial_\alpha\rho+u_\alpha\partial_\beta\rho)+\xi\sum_\gamma u_\gamma\partial_\gamma\rho\delta_{\alpha\beta}. \tag{18}$$

The unknown coefficients $\zeta$, $\xi$ can subsequently be determined in order for Eq. (16) to coincide with the Navier-Stokes equation. The resulting expressions are

$$\zeta=\xi=\nu'=\nu\left(1-4\frac{\partial P}{\partial\rho}\right). \tag{19}$$

A similar result for the nine-bit model but with $\zeta=\nu$ was obtained by Inamuro *et al.* [26] using an asymptotic analysis, and by Holdych *et al.* [25], who considered the terms that involve the pressure derivative with respect to density as negligible. Although this assumption may be valid in many cases, it is evident that the magnitude of the $\partial P/\partial p$ term depends on the state equation and the values of the equation constants. Hence, for the sake of generality, the full expression (16) was considered in the present analysis, leading to the appearance of the $\partial P/\partial p$ term in Eq. (19).

The momentum flux tensor is given by the expression

$$\Pi^{(0)}_{\alpha\beta}=\sum_{i=1}^{6}(\underline{e}_i\underline{e}_i)f_i^{\mathrm{eq}}=P'_{\alpha\beta}+\rho u_\alpha u_\beta. \tag{20}$$

Substituting the equilibrium distribution expansion in the above expression and following algebraic manipulations, it can be shown that the momentum flux tensor can be written as follows:

$$\sum_{i=1}^{6} (\underline{e}_i \underline{e}_i) f_i^{\mathrm{eq}} = P_{\alpha\beta} + \nu'(u_\beta \partial_\alpha \rho + u_\alpha \partial_\beta \rho) + \nu' \sum_\gamma u_\gamma \partial_\gamma \rho \delta_{\alpha\beta} + \rho u_\alpha u_\beta$$

or

$$\begin{aligned} P_{\alpha\beta} + \rho u_\alpha u_\beta &= 3A' \delta_{\alpha\beta} + \tfrac{3}{2}(G'_{\alpha\beta} + C' u_\alpha u_\beta) \\ &\quad - \nu'(u_\beta \partial_\alpha \rho + u_\alpha \partial_\beta \rho) - \nu' \sum_\gamma u_\gamma \partial_\gamma \rho \delta_{\alpha\beta} \\ &= \left(3A' - \nu' \sum_\gamma u_\gamma \partial_\gamma \rho\right) \delta_{\alpha\beta} \\ &\quad + [\tfrac{3}{2} G'_{\alpha\beta} - \nu'(u_\beta \partial_\alpha \rho + u_\alpha \partial_\beta \rho)] + \rho u_\alpha u_\beta . \end{aligned} \tag{21}$$

Using Eq. (12) in index notation, the left-hand side reads

$$P_{\alpha\beta} + \rho u_\alpha u_\beta = \left(p_0 - m\rho\nabla^2\rho - \frac{m}{2}|\nabla\rho|^2\right)\delta_{\alpha\beta} + m\partial_\alpha\rho\partial_\beta\rho + \rho u_\alpha u_\beta . \tag{22}$$

Combining Eqs. (20)–(22), the coefficients of the equilibrium distribution expansion for the Galilean invariant model are obtained (primed quantities),

$$A' = A + \tfrac{2}{3}\nu' \sum_\gamma u_\gamma \partial_\gamma \rho, \tag{23a}$$

$$A'_0 = A_0 - 4\nu' \sum_\gamma u_\gamma \partial_\gamma \rho, \tag{23b}$$

$$B' = B, \quad C' = C, \quad D' = D, \quad D'_0 = D_0,$$

$$G'_{\alpha\alpha} = G_{\alpha\alpha} + \tfrac{2}{3}\nu'(u_\alpha \partial_\alpha \rho - u_\beta \partial_\beta \rho), \tag{23c}$$

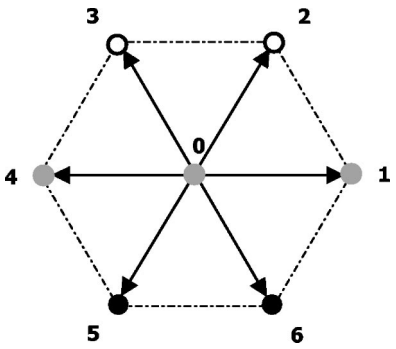


FIG. 1. Solid (filled circles), fluid (open circles), and boundary (gray circles) nodes in the hexagonal lattice.

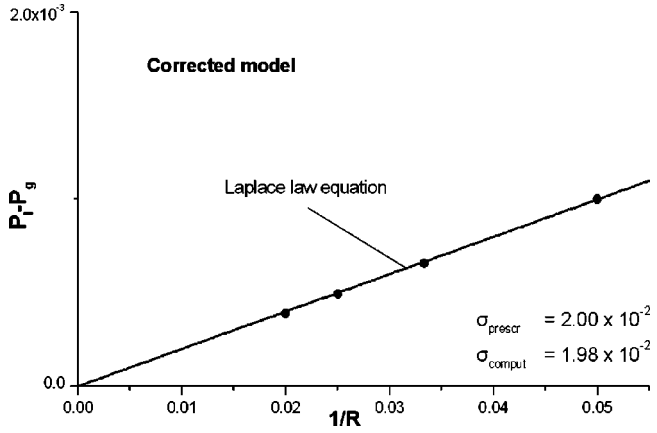


FIG. 2. Laplace law test for a 2D droplet. The solid line represents the Laplace law equation and the symbols indicate the simulation results.

$$G'_{\alpha\beta} = G_{\alpha\beta} + \tfrac{2}{3}\nu'(u_\beta \partial_\alpha \rho + u_\alpha \partial_\beta \rho). \tag{23d}$$

### B. Boundary conditions

Three types of boundary conditions are of relevance here: boundary conditions that induce flow, solid-fluid boundary conditions, and conditions related to the finite size of the working domain. Flow conditions can be implemented in two ways: a pressure (or density) gradient can be imposed in the desired direction of flow, or the velocity can be prescribed at the inlet or outlet of the system. Periodic boundary conditions allow populations leaving the working domain to reenter in the same direction through the opposite boundaries.

There are several types of solid-fluid boundary conditions that can be used in LB models, including the typical ''bounce-back'' condition and also some more complicated ones [29]. In our computations, both the ''bounce-back'' and a ''relaxed bounce-back'' condition have been tested. The latter is an improved ''bounce-back'' condition imposed at the boundary nodes, which are also assumed to suffer colli-

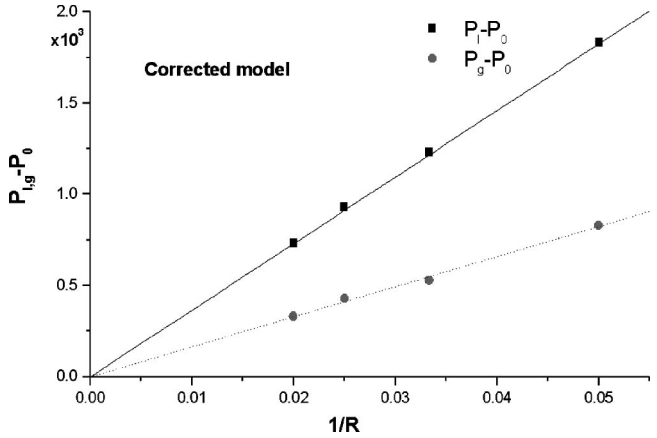


FIG. 3. Comparison of the simulated pressure differences (liquid, vapor) from the common pressure for a flat interface (symbols), with the theoretical calculations from the Gibbs-Thomson equations (solid lines).

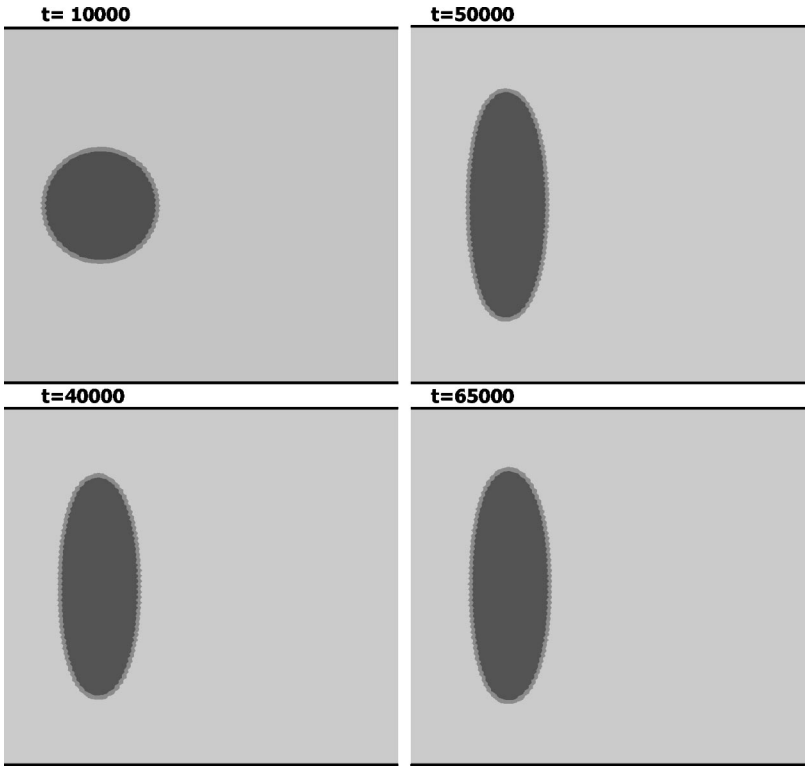


FIG. 4. Simulation of a moving tube containing an initially circular droplet in equilibrium with its vapor. The original 2D two-phase model was used. The parameter values are $\nu_l=\nu_g=0.125$, $kT=0.37$, $m=0.015$, the corresponding densities of the two phases are $\rho_l=4.895$, $\rho_g=2.211$, and the corresponding surface tension is $\sigma=0.02$. $N_{\mathrm{Re}}=105$.

sions. Nevertheless, use of one or the other condition has no discernible effect on the flow field provided that $\tau \leqslant 1$. For moving walls, a ''no-slip'' constraint [30] is imposed on the fluid populations that are immediately adjacent to the solid surface. The unknown distribution functions, directed from the solid sites into the fluid, are calculated from the local macroscopic density ($\rho$) and momentum ($\rho \underline{u}$) equations,

$$\rho = \sum_i f_i , \tag{24}$$

$$\rho \underline{u} = \sum_i \underline{e}_i f_i . \tag{25}$$

For instance, the unknown populations in Fig. 1 move in directions 2, 3 ($f_2, f_3$). The density at the boundary node is

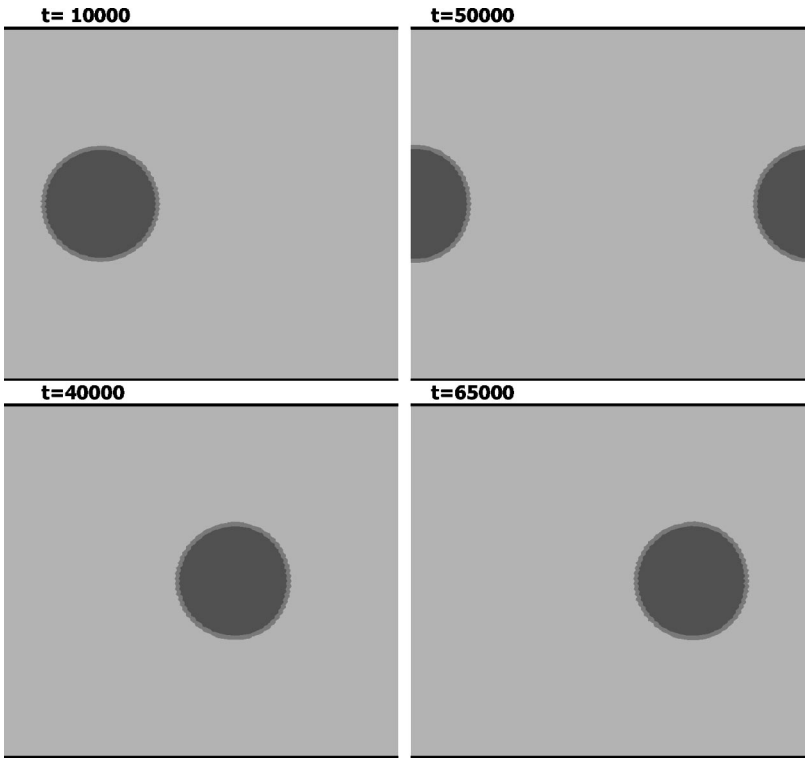


FIG. 5. Simulation of a moving tube containing an initially circular droplet in equilibrium with its vapor. The corrected for Galilean invariance 2D two-phase model was used. The parameter values are the same as those used in Fig. 4. $N_{\mathrm{Re}}=105$.

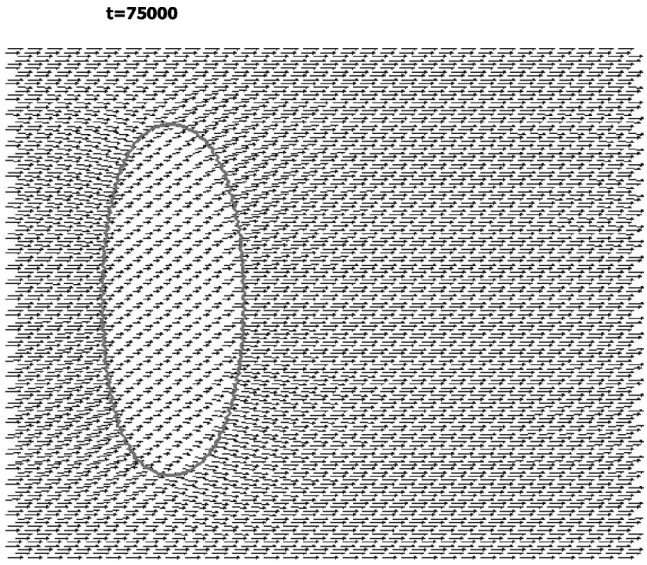


FIG. 6. Velocity field in and around a droplet in a moving tube, using the original 2D two-phase model. The parameter values are the same as those used in Fig. 4.

also to be calculated. If the wall is impermeable, the $y$ component of the velocity ($u_y$) is zero. Once the horizontal velocity component ($u_x$) is set to the desired value of the wall velocity, the unknown local populations can be calculated from the following set of equations:

$$\rho = f_0 + f_1 + f_2 + f_3 + f_4 + f_5 + f_6, \tag{26a}$$

$$\rho u_x = f_1 - f_4 + \tfrac{1}{2}(f_2 + f_6 - f_3 - f_5), \tag{26b}$$

$$\rho u_y = \tfrac{\sqrt{3}}{2}(f_2 + f_3 - f_5 - f_6) = 0. \tag{26c}$$

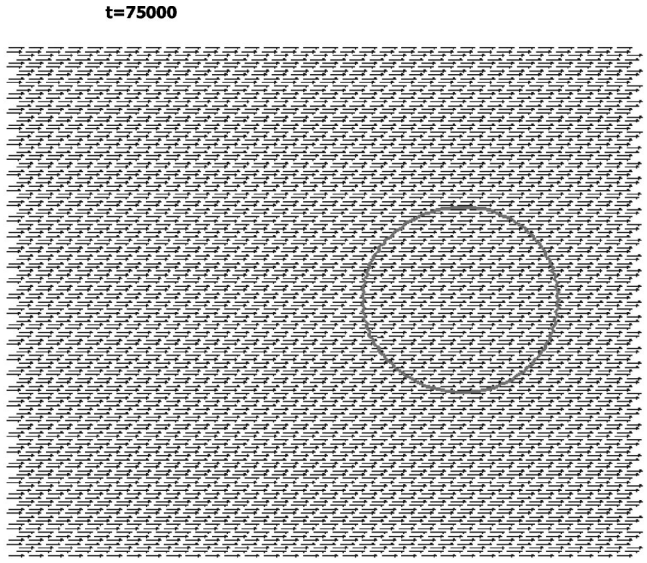


FIG. 7. Velocity field in and around a droplet in a moving tube, using the 2D two-phase model, corrected for Galilean invariance. The parameter values are the same as those used in Fig. 4.

## III. RESULTS AND DISCUSSION

### A. Equilibrium simulations

Before using the Galilean-invariant model in flow simulations, some basic validation runs are performed. First, a droplet at equilibrium with its vapor is simulated in the absence of external flow field. The grid size is $128\times128$ lattice sites and periodic boundary conditions are employed around the working domain. The input data are $\nu_l=\nu_g=0.125$, $kT=0.55$, $m=0.01$, and $\rho_l=4.895$, $\rho_g=2.211$. Following the algorithm proposed by Angelopoulos *et al.* [19] and the discussion made in Sec. II, the corresponding van der Waals coefficients are $a=\frac{9}{49}$, $b=\frac{2}{21}$, the interface thickness is $D=2.385$, and the corresponding surface tension is $\sigma=0.02$. The pressure difference across the interface is calculated after about 40 000 time steps to ensure that the system is fully equilibrated. In Fig. 2 the pressure difference is plotted against the droplet curvature. The continuous line represents the Laplace law for the prescribed surface tension ($\sigma=0.02$). An excellent agreement is noted, the maximum relative error between the prescribed surface tension and the calculated one being less than 1%.

Another test of thermodynamic consistency of the model is presented in Fig. 3. The quantities $P_l-P_0$ and $P_g-P_0$ are plotted against the droplet curvature, where $P_l$ is the liquid pressure, $P_g$ is the gas pressure, and $P_0$ is the corresponding pressure for a flat interface. The parameter values are the same as those in the Laplace law test and the grid size is $128\times128$ lattice sites. The theoretical values of the aforementioned pressure differences are calculated from the Gibbs-Thomson equations and represented with the solid and dashed lines for the liquid and gas phases, respectively,

$$P_l = P_0 + \frac{\rho_l}{\rho_l - \rho_g}\frac{\sigma}{R}, \tag{27a}$$

$$P_g = P_0 + \frac{\rho_g}{\rho_l - \rho_g}\frac{\sigma}{R}. \tag{27b}$$

Again, an excellent agreement between the theoretical and the calculated values is obtained.

The spurious currents in the interface region are slightly reduced upon restoration of the Galilean invariance. It was found that for a droplet at equilibrium with its vapor ($\nu_l=\nu_g=0.125, kT=0.37$, $m=0.015$, $\rho_l=4.895$, $\rho_g=2.211$, $\sigma=0.02$) the mean magnitudes of these velocities in the two cases are $0.4\times10^{-3}$ and $0.35\times10^{-3}$, respectively, while the corresponding maximum values are $1.0\times10^{-3}$ and $0.8\times10^{-3}$. These values are quite small given that the spurious currents in the original van der Waals LB model were already reduced by three orders of magnitude compared to those in the two-phase LB model by Shan and Chen [14], which, in turn, were lower [31] than the LG model proposed by Rothman and Keller [6] or the corresponding LB model proposed by Gustensen *et al.* [7] and Grunau, Chen, and Eggert [11].

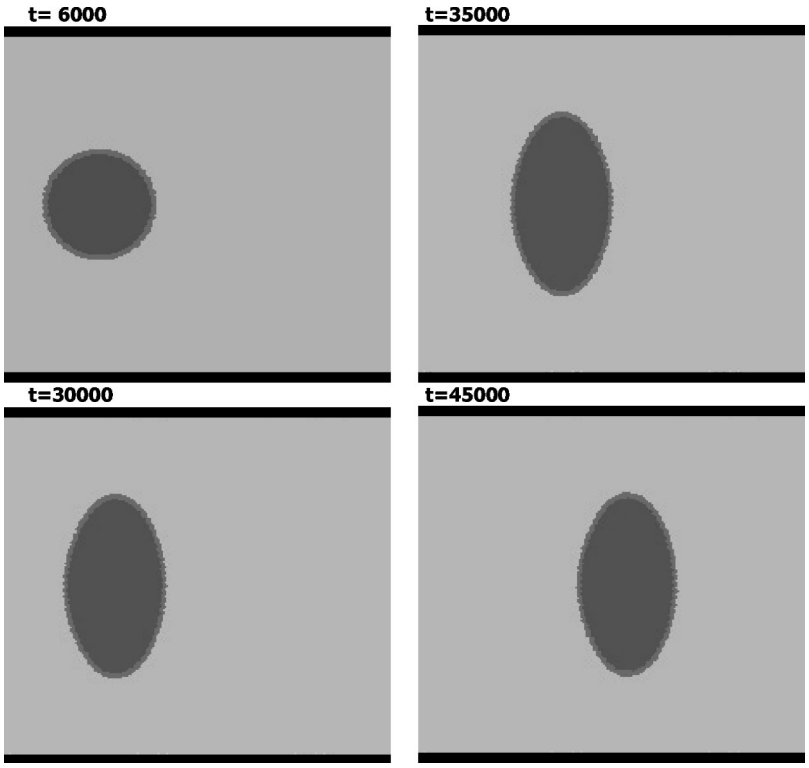


FIG. 8. Simulation of droplet motion in a stationary tube, subject to an externally applied pressure drop. The original 2D two-phase model was used. The parameter values are the same as those used in Fig. 4. $N_{\mathrm{Re}}=100$.

### B. Flow simulations

Flow simulations were carried out to demonstrate the practical significance of the Galilean-invariance restoration in simple two-phase systems. Figures 4 and 5 show simulated snapshots of a moving tube that contains an initially circular droplet, using the original model, which lacks Galilean invariance, and the corrected model, respectively. The solid-fluid ''no-slip'' boundary condition mentioned in the preceding section was used. The velocity in the direction of the tube motion ($u_x$) was set equal to 0.1, whereas the velocity component normal to the wall ($u_y$) was set equal to zero. Periodic boundary conditions were employed in the

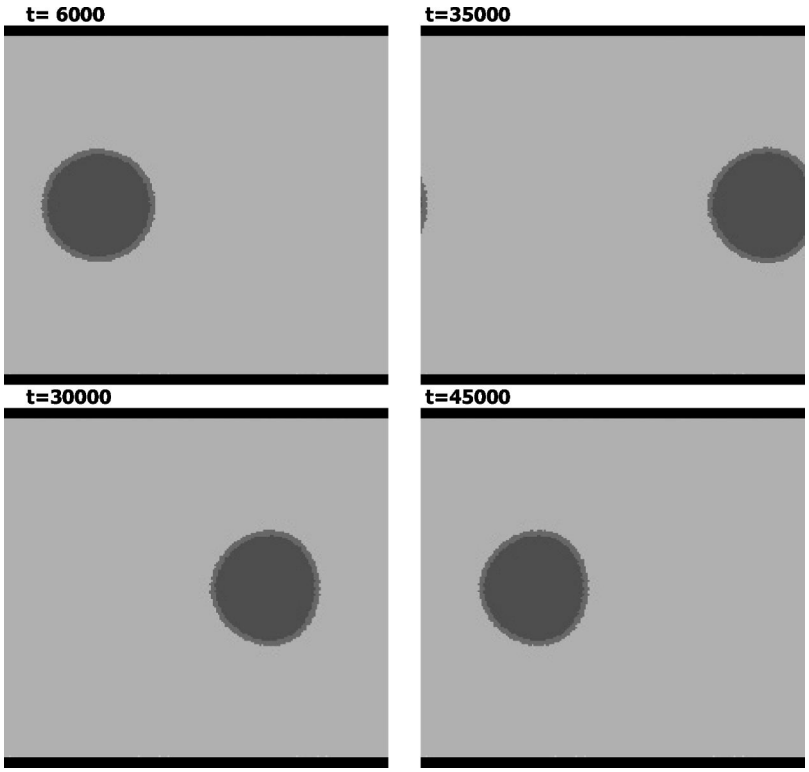


FIG. 9. Simulation of droplet motion in a stationary tube, subject to an externally applied pressure drop. The corrected 2D two-phase model was used. The parameter values are the same as those used in Fig. 4. $N_{\mathrm{Re}}=100$.

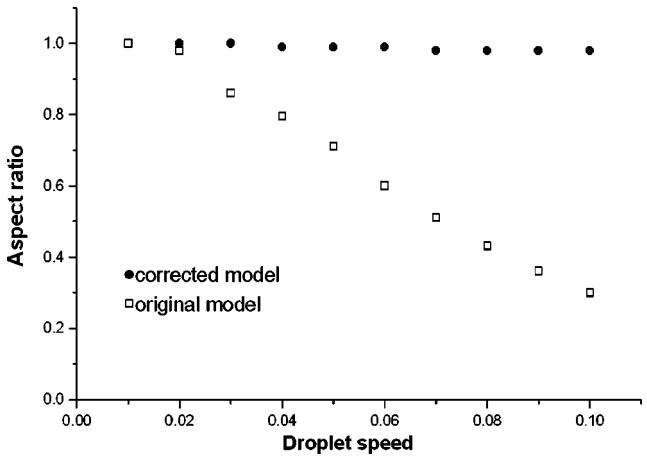


FIG. 10. Aspect ratio (size in the direction of flow to size in the transverse direction) of droplet moving in the absence of walls vs droplet velocity. Despite the use of a moving coordinate system, the droplet shape remains, practically, unaffected when the corrected model is used (Galilean invariance is restored). The parameter values are $\nu_l=0.125$, $\nu_g=0.125$, $m=0.015$, $kT=0.37$, $\sigma=0.02$, and the corresponding densities are $\rho_l=4.895$, $\rho_g=2.211$.

direction of the tube motion. The grid size is $128\times135$ lattice sites and the Reynolds number is $N_{\mathrm{Re}}=d\langle u_x\rangle/\nu_l=105$, where $d$ is the tube diameter and $\langle u_x\rangle$ is the mean value of the $x$ component of the velocity, calculated at the tube entrance. Figure 4 shows that the lack of Galilean invariance leads to strong deformation of the droplet, which assumes eventually an elliptic shape with aspect ratio equal to 3. The droplet appears to be very slightly affected by the tube motion and by the concomitant flow that develops, and eventually comes to rest. On the contrary, Fig. 5 shows that the model allows the droplet to retain its initial shape and to undergo a smooth motion along the mean flow direction. Figures 6 and 7 show the corresponding velocity profiles using the original and the corrected model, respectively. In the former case, the droplet acts as an obstacle to the gas flow, moving at a largely different speed from that of the tube, whereas in the latter case the droplet has acquired the speed of the tube wall.

Similar results are obtained in flows driven by an externally applied pressure drop. The tube wall is held stationary and, consequently, the ''no-slip'' solid-fluid boundary condition is used, as mentioned in Sec. II. The grid size is $100\times107$ lattice sites. The parameter values are the same as those in the moving tube case. Simulated snapshots using the original and the corrected model are shown in Figs. 8 and 9, respectively. Again, lack of Galilean invariance leads to an elliptic shape with aspect ratio being equal to 1.8, whereas the droplet remains circular in the corrected model. Along the inlet face (left end), momentum is added to the populations that enter the tube, at a rate that is proportional to the prescribed pressure gradient. The populations that exit the tube through the inlet face set the corresponding populations that enter through the exit face (periodic boundary condition). In the absence of walls, the original model predicts that the aspect ratio of the droplet decreases rapidly with increasing flow rate or, equivalently, with increasing speed of the coordinate system that moves along with the droplet (Fig. 10). However, restoration of the Galilean invariance removes this artifact and leaves the droplet shape practically unaffected by the droplet speed.

### C. Jet dynamics

Jet instability and droplet formation have been studied using a variety of numerical techniques, including finite differences, finite elements, and finite volumes. Recently, lattice-Boltzmann schemes for incompressible multiphase flows have been developed in order to simulate the Rayleigh-Taylor instability and the concomitant droplet formation [32,33]. It is beyond the scope of the present work to review this literature or to assess the performance of the various

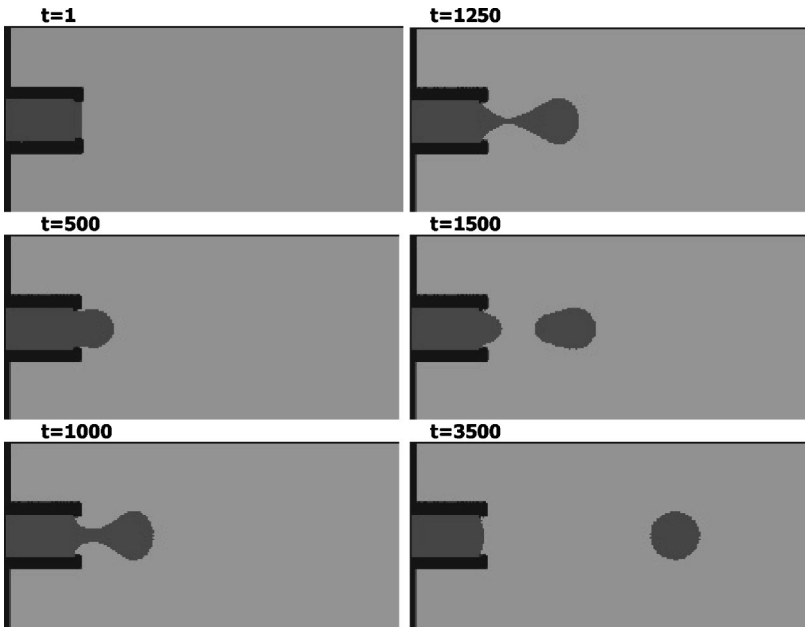


FIG. 11. Simulation of droplet generation from an orifice, using the model proposed in this work. The parameter values are $\nu_l=0.02$, $\nu_g=0.05$, $m=10^{-3}$, $kT=4.56\times10^{-3}$, $\sigma=6.88\times10^{-2}$, the corresponding densities are $\rho_l=20$, $\rho_g=1$, and the reduced temperature is $T/T_c=0.68$. $N_{\mathrm{Re}}=78$.

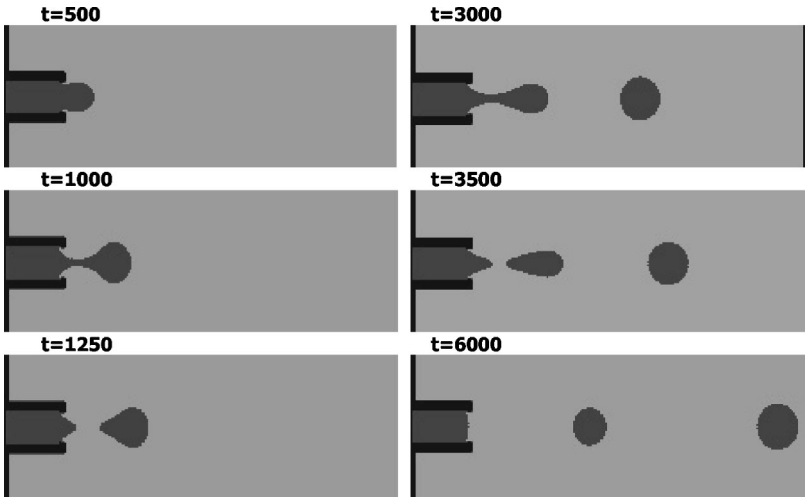


FIG. 12. Simulation of sequential droplet generation from an orifice, using the model proposed in this work. The parameter values are the same as those used in Fig. 11.

computational techniques. Instead, it is very interesting to demonstrate here the capability of the LB two-phase model, corrected for Galilean invariance, to simulate the main jet-related phenomena, without resorting to any assumption regarding the initial shape of the jet or to an artificial perturbation that would induce instability, as is typically done in the literature.

A straight nozzle with a slightly narrowed tip is assumed in our jet simulations; however, the use of any other shape is quite trivial in LB techniques in contrast to other numerical methods. A simple ''bounce-back'' boundary condition has been used at the solid-fluid interface. The wettability condition at the nozzle wall is known to play significant role in jet dynamics. The desired wettability can be tuned by assigning a desired profile of chemical potential $\mu_w(\underline{r})$ to the walls. Gradients of the chemical potential act as a thermodynamic force on the fluid [15]. Alternatively, gradients of chemical potential can be imposed by assigning a density profile $\rho_w(\underline{r})$ to the solid sites, which corresponds to a chemical potential profile according to the following expression:

$$\mu(\rho,T)=kT\ln\frac{\rho}{1-b\rho}+\frac{kT}{1-b\rho}-2a\rho \tag{28}$$

as explained by Angelopoulos *et al.* [19].

An abrupt change of the contact angle at the nozzle tip may affect critically the droplet formation stage and, in particular, the droplet size and shape, as well as the time to breakup. Figure 11 presents simulated snapshots of droplet formation using the corrected two-phase model. The grid size is $200\times100$ lattice sites; the nozzle diameter contains 25 sites; the nozzle tip contains 21 sites; and the nozzle length extends to 39 sites. Initially, the nozzle is filled with liquid, whereas the rest of the working domain is filled with vapor, as shown in the first snapshot. The nozzle is assumed liquid wet, in contrast to the tip, which is strongly gas (vapor) wet. Periodic boundary conditions are employed along the top and bottom sides of the simulated region, as explained in Sec. II.

At the nozzle inlet, time dependent flow conditions may be imposed to simulate the periodic forcing profile used in

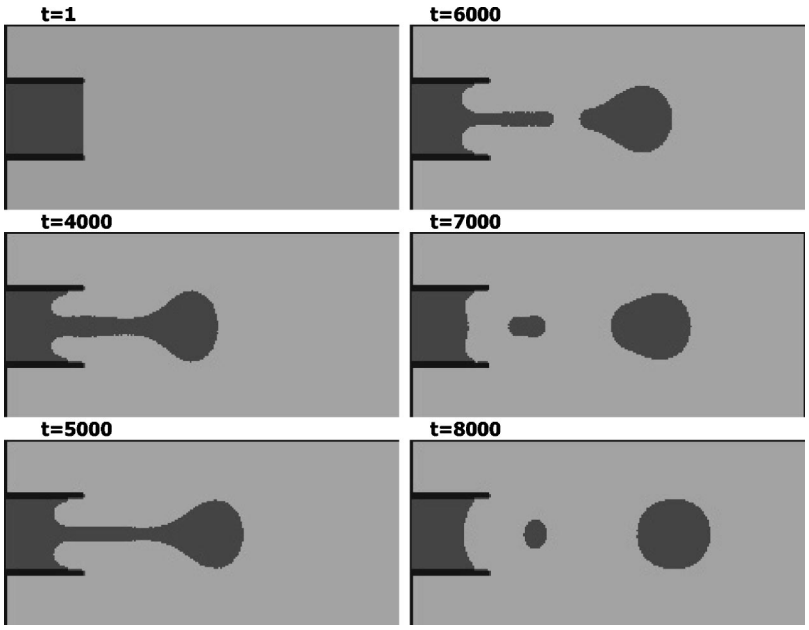


FIG. 13. Simulation of satellite droplet formation, using the model proposed in this work. The parameter values are $\nu_l=0.06$, $\nu_g=0.01$, $m=1.25\times10^{-3}$, $kT=2.6\times10^{-3}$, $\sigma=1.35\times10^{-2}$, the corresponding densities are $\rho_l=10$, $\rho_g=1$, and the reduced temperature is $T/T_c=0.77$. $N_{\mathrm{Re}}=62$.

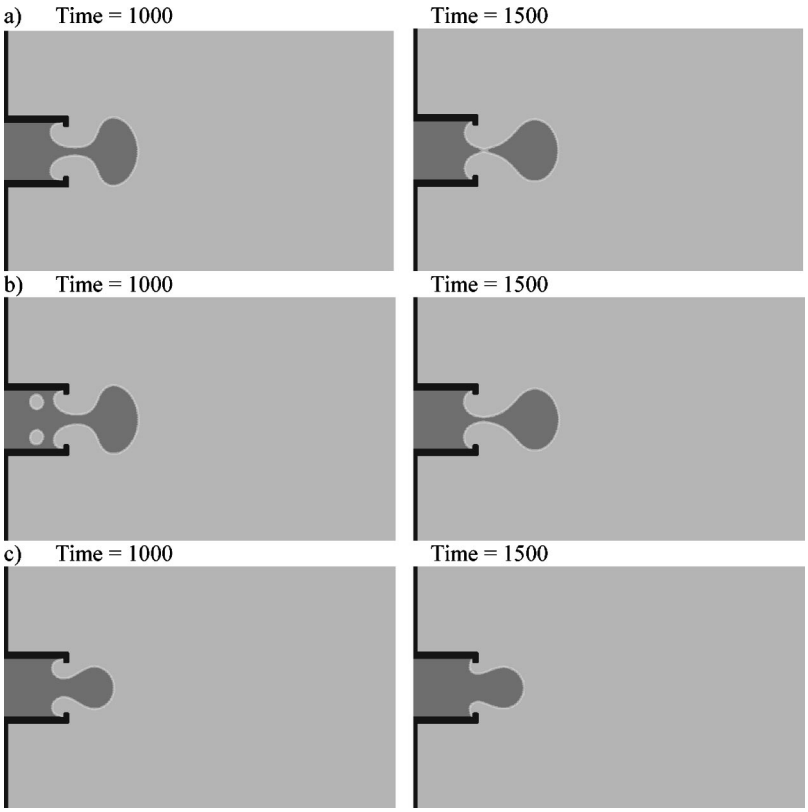


FIG. 14. Jet simulation using (a) the model proposed in this work, (b) an approximate Galilean restoration procedure that neglects certain pressure terms, (c) the original, untreated model. The parameter values are $\nu_l=\nu_g=0.125$, $m=0.01$, $kT=0.55$, $\sigma=0.02$, the corresponding densities are $\rho_l=4.895$, $\rho_g=2.211$, and the reduced temperature is $T/T_c=0.55$. $N_{\mathrm{Re}}=38$. Charge period: 265 time steps. Lattice size: $300\times200$.

ink-jet printing. In the present simulation runs, the constant ''charge'' stage lasts 500 time steps, followed by a ''rest'' stage. During the ''charge'' stage, the momentum of the populations entering the nozzle in the mean flow direction is increased 400 times per site to induce flow, for all sites along the first single column inside the nozzle. At the right boundary of the working domain it is assumed that $\partial_x u_x=0$.

It is noteworthy that the simulator captures a number of phenomena that relate to droplet formation: generation of a liquid meniscus, necking, gradual thinning of neck, thread snap-off, droplet rounding, and eventually droplet motion away from the orifice. It must be stressed that the original model, that is, the one that does not preserve Galilean invariance, fails to reproduce droplet motion once formed. Instead, the droplet assumes an elliptic shape, just as the one shown in Fig. 8, and remains stationary.

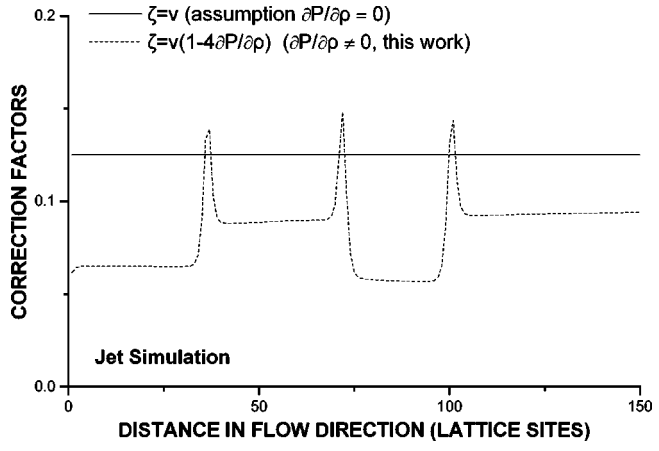


FIG. 15. Variation of the correction factor used in this work in the jet direction for the case of Fig. 14(a) at time=1000. Distance from the lower nozzle wall: 1/5 nozzle width. Comparison with the correction factor suggested by an approximate Galilean restoration procedure that neglects pressure terms.

If a second ''charge'' stage is employed following the ''rest'' stage, a second droplet is generated (Fig. 12). The parameter values are the same as those used in Fig. 11, though the grid size is $250\times100$ to provide more space for the motion of the first droplet. The ''rest'' stage lasts 1000 time steps and the duration of the second ''charge'' stage is equal to that of the first ''charge'' stage, i.e., 500 time steps. The momentum of the populations entering the nozzle in the first ''charge'' stage is increased 450 times to induce flow, but the corresponding increase in the second ''charge'' stage is only 360. Due to that, the second droplet is smaller than the first one, in accord with the relevant observations made during actual ink-jet operation. It is also worth noting that the simulator can follow the motion of both droplets in the direction of momentum addition, in contrast to the original, noncorrected model.

The formation of satellite droplets during liquid ejection from an orifice is of strong scientific and technological interest, especially to ink-jet technologies and related applications, as it may affect severely the printing quality. Figure 13 shows that the present simulator, corrected for Galilean invariance, can reproduce this phenomenon in a quite realistic manner. The wettability of the nozzle tip was modified, following a procedure adopted in ink-jetting practice, so that the outer portion of the tip is wetted preferentially by the

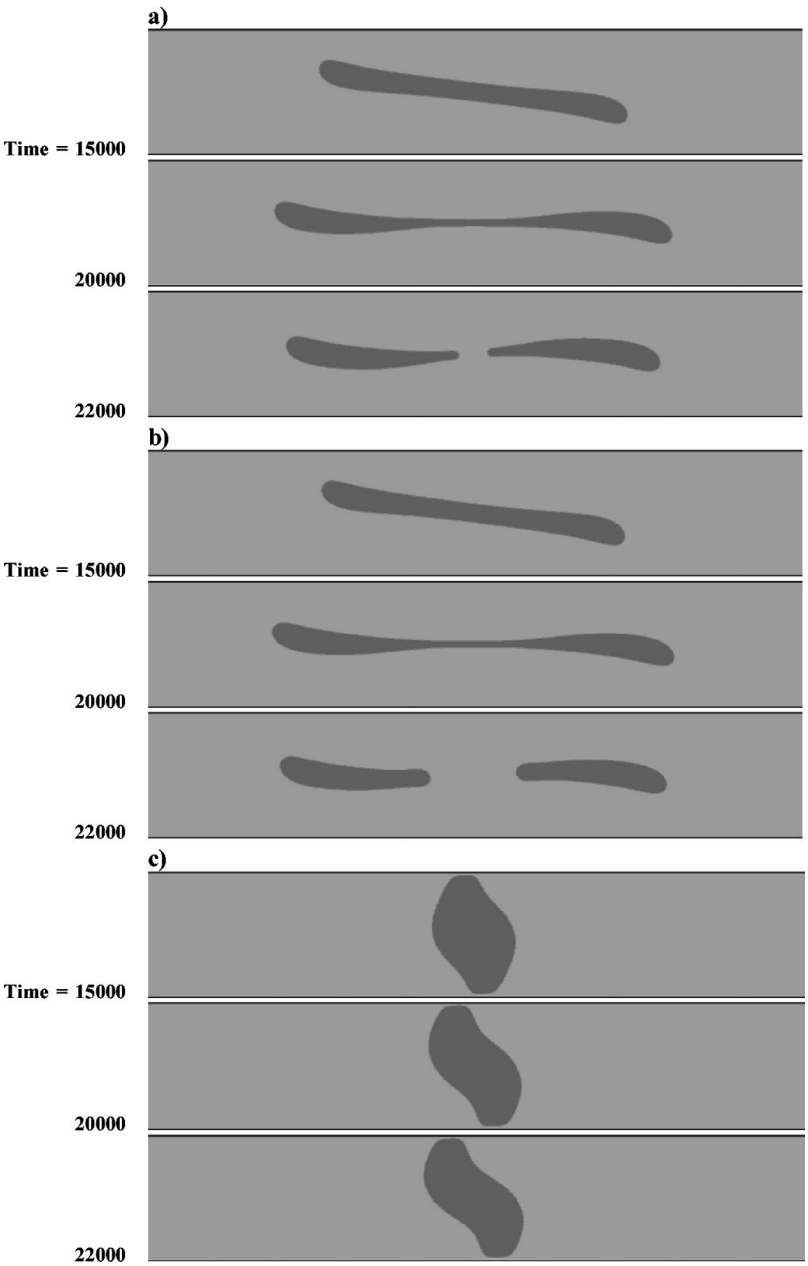


FIG. 16. Shear flow conditions imposed on a droplet by the opposite direction of the top and bottom walls at speed $u=0.11$. Simulation results using (a) the model proposed in this work, (b) an approximate Galilean restoration procedure that neglects certain pressure terms, (c) the original, untreated model. The parameter values are $\nu_l=\nu_g=0.125$, $m=0.01$, $kT=0.55$, $\sigma=0.02$, and the corresponding densities are $\rho_l=4.895$ and $\rho_g=2.211$. Lattice size: $500\times101$.

vapor phase. One way to achieve this is by maintaining a vapor ''layer'' there, which facilitates the formation of a neck well inside the nozzle region. The neck is elongated until it ruptures at two points: first upfront, thus creating the main droplet and, later, in the region of contact with the bulk liquid. The secondary droplet is then deformed, subject to the action of the surface tension and, eventually, rounds up and travels in the vapor phase, following the primary droplet. The resemblance of the simulated snapshots to those computed using a finite elements technique [34] (which is, however, confined to the stage prior to interface rupture in contrast to the present method) is quite impressive. It is reasonable to expect that simulations of this type can shed light to the conditions for satellite droplet formation in real systems and, possibly, guide the design of improved ink-jet processes.

Some useful remarks on the methodology for the restoration of Galilean invariance are in order next. The approach used in this work takes into consideration all the terms that arise in the momentum equation prior to the correction procedure. Excluding the pressure-dependent terms on the right-hand side of Eq. (9) from the Galilean-invariance restoration procedure would certainly simplify the analysis, leading to simple expressions for the expansion coefficients. Specifically, Eqs. (23) would in that case involve only the kinematic viscosity $\nu$ in place of the $\zeta$ factor, defined in Eq. (19). However, this approximation may not be always accurate. For instance, Fig. 14 shows that adoption of such a simplification in a typical jet simulation could give rise to a different flow pattern from that obtained by the full analysis. Nevertheless, it is clear that both approaches perform considerably different from the original approach [Fig. 14(c)], that is, from the approach that uses the untreated pressure tensor. The deviation of the flow pattern of Fig. 14(b) from that of Fig. 14(a)

can be traced to the different correction factors used in the two approaches. Figure 15 shows an interesting variation of the $\zeta$ factor in the jet direction, as results from the application of the full analysis (dashed curve). On the other hand, the simplified version of the Galilean-invariance restoration procedure would require a constant value for $\zeta$ (namely, $\zeta = \nu$, solid line), which may alter the values of the expansion coefficients $A'$, $A'_0$, $G'_{\alpha\alpha}$, and $G'_{\alpha\beta}$, affecting, thus, the flow calculations.

Figure 16 shows that the use of constant or variable $\zeta$ may result in different flow configurations even in simpler cases. Shear flow conditions are induced by the motion of the top and bottom walls in opposite directions. The droplet is initially allowed to relax for 10 000 time steps. Direct comparison of snapshots taken at the same time instants using (a) the model presented here with $\zeta$ given from Eq. (19), (b) the simplified Galilean restoration model that uses $\zeta = \nu$, and (c) the original uncorrected model, reveals that the first two models lead to similar, but not identical, configurations—attained with a time lag—which are quite different from the configuration predicted by the uncorrected model.

## IV. CONCLUSIONS

A Galilean-invariant two-dimensional (2D) lattice-Boltzmann model, capable of simulating two-phase systems is presented in this work. The model is based on the original work of Swift, Osborn, and Yeomans [15] though the Navier-Stokes equation is fully recovered here and Galilean invariance is preserved, thanks to an appropriate reformulation of the motion equation and a modified form of the pressure tensor. Once the basic model is developed, one can use the algorithm proposed by Angelopoulos *et al.* [19] for the prescription of the desired fluid properties, including viscosities, surface tension, and temperature.

Simulation tests have been performed to validate the model. Excellent agreement between the static droplet simulation results with both the Laplace law and the Gibbs-Thomson equations was obtained. A number of flow simulations involving liquid-vapor interfaces were carried out and the importance of restoring the Galilean invariance was demonstrated. In contrast to its predecessors, the simulator presented here suppresses undesirable droplet deformation and reproduces known flow scenarios in straight tubes.

The proposed simulator was also used for the study of jet break-up and droplet generation, adopting the approach of simple momentum addition at the entrance of a straight nozzle. It was seen that the simulator is capable of capturing all the main events that are known to occur during liquid ejection and droplet formation, without having to resort to any external disturbances to induce jet instability. The simulator is also sufficiently stable to treat the singularity that develops at snap-off, in contrast to other numerical schemes that can be used either before or after snap-off. Variable wettability can also be implemented in a simple way by just adjusting the local chemical potential or, alternatively, the density on the solid-fluid boundaries.

As a general conclusion, it can be stated that the present model can be very useful in the study of interfaces under both static and flow conditions. Its main contribution is towards understanding some key mechanisms that underlie interface stability, deformation, and propagation during two-phase flow and phase separation. Nonetheless, the employment of this approach to actual technological problems, like ink-jet printing, requires the development of its 3D version, which is already in progress by the authors.

## ACKNOWLEDGMENTS

This work was supported financially by EPSON-SEIKO Corporation and by the Institute of Chemical Engineering and High Temperature Chemical Processes—Foundation for Research and Technology, Hellas (ICE/HT-FORTH).

[1] U. Frisch, B. Hasslacher, and Y. Pomeau, Phys. Rev. Lett. **56**, 1505 (1986).
[2] U. Frisch, D. d'Humieres, B. Hasslacher, P. Lallemand, Y. Pomeau, and J. P. Rivet, Complex Syst. **1**, 649 (1987).
[3] Y. H. Qian, Ph.D. thesis, University of Paris, 1990; Y. Qian, D. d'Humieres, and P. Lallemand, Europhys. Lett. **17**, 479 (1992).
[4] S. Chen, H. Chen, D. Martinez, and W. H. Matthaeus, Phys. Rev. Lett. **67**, 3776 (1991); H. Chen, S. Chen, and W. H. Matthaeus, Phys. Rev. A **45**, 5339 (1992).
[5] P. L. Bhatnagar, E. P. Gross, and M. Krook, Phys. Rev. **94**, 511 (1954).
[6] D. Rothman and J. M. Keller, J. Stat. Phys. **52**, 119 (1988).
[7] A. K. Gustensen, D. H. Rothman, S. Zaleski, and G. Zanetti, Phys. Rev. A **43**, 4320 (1991).
[8] A. K. Gustensen and D. H. Rothman, Europhys. Lett. **18**, 157 (1992).
[9] I. Ginzbourg and P. M. Adler, Transp. Porous Media **20**, 37 (1995).
[10] D. Grunau, Ph.D. thesis, Colorado State University, 1993.
[11] D. Grunau, S. Chen, and K. Eggert, Phys. Fluids A **5**, 2557 (1993).
[12] C. Appert and S. Zaleski, Phys. Rev. Lett. **64**, 1 (1990); J. Phys. II **3**, 309 (1993).
[13] C. Appert, D. D'Humieres, V. Pot, and S. Zaleski, Transp. Theory Stat. Phys. **23**, 107 (1994).
[14] X. Shan and H. Chen, Phys. Rev. E **47**, 1815 (1993); **49**, 2941 (1994).
[15] M. R. Swift, W. R. Osborn, and J. M. Yeomans, Phys. Rev. Lett. **75**, 830 (1995).
[16] M. R. Swift, E. Orlandini, W. R. Osborn, and J. M. Yeomans, Phys. Rev. E **54**, 5041 (1996).
[17] J. W. Cahn and J. E. Hilliard, J. Chem. Phys. **28**, 258 (1958).
[18] J. S. Rowlinson and B. Widom, *Molecular Theory of Capillarity* (Clarendon, Oxford, 1982).
[19] A. D. Angelopoulos, V. N. Paunov, V. N. Burganos, and A. C.

Payatakes, Phys. Rev. E **57**, 3237 (1998).
[20] X. He and L. Luo, Phys. Rev. E **55**, 6333 (1997); **56**, 6811 (1997).
[21] L. Luo, Phys. Rev. Lett. **81**, 1618 (1998).
[22] T. Abe, J. Comput. Phys. **131**, 241 (1997).
[23] S. Chapman and T. G. Cowling, *The Mathematical Theory of Non-Uniform Gases* (Cambridge University, London, 1970).
[24] X. He, X. Shan, and G. D. Doolen, Phys. Rev. E **57**, R13 (1998).
[25] D. J. Holdych, D. Rovas, J. G. Georgiadis, and R. O. Buckius, Int. J. Mod. Phys. C **9**, 1393 (1998).
[26] T. Inamuro, N. Konishi, and F. Ogino, Comput. Phys. Commun. **129**, 32 (2000).
[27] R. Evans, Adv. Phys. **28**, 143 (1979).
[28] J. D. Sterling and S. Chen, J. Comput. Phys. **123**, 196 (1996).
[29] O. Behrend, Phys. Rev. E **52**, 1164 (1995).
[30] D. R. Noble, S. Chen, J. G. Georgiadis, and R. O. Buckius, Phys. Fluids **7**, 203 (1995).
[31] S. Hou, X. Shan, Q. Zou, G. D. Doolen, and W. E. Soll, J. Comput. Phys. **138**, 695 (1997).
[32] X. He, Y. H. Qian, G. D. Doolen, and S. Chen, Phys. Rev. E **58**, 6861 (1998); X. He, S. Chen, and R. Zhang, J. Comput. Phys. **152**, 642 (1999); X. He, R. Zhang, S. Chen, and G. D. Doolen, Phys. Fluids **11**, 1143 (1999).
[33] H. Xi and C. Duncan, Phys. Rev. E **59**, 3022 (1999).
[34] E. D. Wilkes, S. D. Phillips, and O. A. Basaran, Phys. Fluids **11**, 3577 (1999).